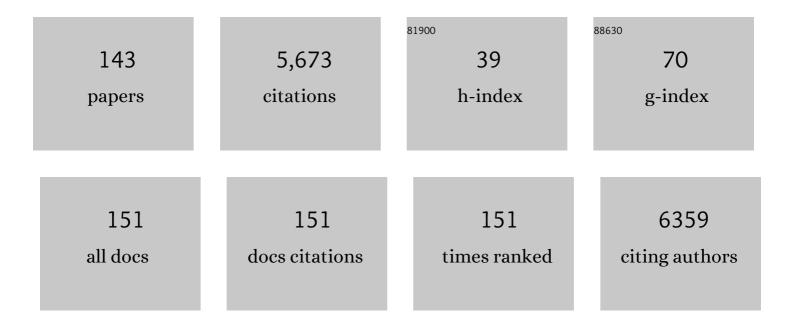
List of Publications by Year in descending order

Source: https://exaly.com/author-pdf/5628857/publications.pdf Version: 2024-02-01



#	Article	IF	CITATIONS
1	Role of Fe2Al5 in fracture of novel dissimilar aluminum-steel resistance spot welds using multi-ring domed electrodes. Materials Science & Engineering A: Structural Materials: Properties, Microstructure and Processing, 2022, 831, 142233.	5.6	18
2	Indentation strain rate sensitivity of laser-powder bed fused and electron beam melted Ti–6Al–4V. Vacuum, 2022, 195, 110690.	3.5	5
3	Synthesis of In Situ SiC/Graphite/Al Hybrid Composite Coating by Laser Direct Energy Deposition. Metallurgical and Materials Transactions A: Physical Metallurgy and Materials Science, 2022, 53, 484-502.	2.2	1
4	Microstructural-micromechanical correlation in an Al–Cu–Mg–Ag–TiB2 (A205) alloy: additively manufactured and cast. Materials Science & Engineering A: Structural Materials: Properties, Microstructure and Processing, 2022, 832, 142453.	5.6	26
5	Characterization and statistical modeling of texture and microstructure evolution in dynamically fractured electron beam melted Ti-6Al-4V. Materialia, 2022, 21, 101342.	2.7	1
6	Microstructural Evolution in Additively Manufactured Fe-Cr-Ni Maraging Stainless Steel. Metallurgical and Materials Transactions A: Physical Metallurgy and Materials Science, 2022, 53, 1771-1792.	2.2	4
7	Microstructure Modelling of the HEC Behaviour of a Novel Vanadium DP980 Cold Rolled Alloy. Minerals, Metals and Materials Series, 2022, , 909-920.	0.4	1
8	On the bending of MS1-P20 hybrid steels additively manufactured using laser powder bed fusion. Materialia, 2022, 24, 101501.	2.7	3
9	On the microstructure and solidification behavior of new generation additively manufactured Al-Cu-Mg-Ag-Ti-B alloys. Additive Manufacturing, 2021, 37, 101724.	3.0	15
10	Plastic deformation throughout strain-induced phase transformation in additively manufactured maraging steels. Materials and Design, 2021, 198, 109289.	7.0	32
11	Texture evolution in selective laser melted maraging stainless steel CX with martensitic transformation. Journal of Materials Science, 2021, 56, 844-853.	3.7	22
12	Concurrent improvement of strength and ductility in heat-treated C300 maraging steels produced by laser powder bed fusion technique. Additive Manufacturing, 2021, 39, 101847.	3.0	12
13	Atom probe tomography study of \hat{I}^{2} -phases in additively manufactured nickel aluminum bronze in as-built and heat-treated conditions. Materials and Design, 2021, 202, 109541.	7.0	26
14	Corrosion resistance of 13wt.% Cr martensitic stainless steels: Additively manufactured CX versus wrought Ni-containing AISI 420. Corrosion Science, 2021, 184, 109362.	6.6	41
15	A relationship between the build and texture orientation in tensile loading of the additively manufactured maraging steels. Additive Manufacturing, 2021, 41, 101954.	3.0	6
16	The effect of chemical patterning induced by cyclic plasticity on the formation of precipitates during aging of an Al–Mg–Si alloy. Materials Science & Engineering A: Structural Materials: Properties, Microstructure and Processing, 2021, 815, 141265.	5.6	14
17	Additive manufactured versus cast AlSi10Mg alloy: Microstructure and micromechanics. Results in Materials, 2021, 10, 100178.	1.8	40
18	A new route for developing ultrafine-grained Al alloy strips using repetitive bending under tension. Materials and Design, 2021, 206, 109750.	7.0	4

#	Article	IF	CITATIONS
19	A hybrid additively manufactured martensitic-maraging stainless steel with superior strength and corrosion resistance for plastic injection molding dies. Additive Manufacturing, 2021, 45, 102068.	3.0	8
20	Corrosion performance of additively manufactured bimetallic aluminum alloys. Electrochimica Acta, 2021, 389, 138689.	5.2	6
21	Microstructural consistency in the additive manufactured metallic materials: A study on the laser powder bed fusion of AlSi10Mg. Additive Manufacturing, 2021, 46, 102166.	3.0	9
22	Indentation-derived mechanical properties of Ti-6Al-4V: Laser-powder bed fusion versus electron beam melting. Materials Letters, 2021, 301, 130273.	2.6	14
23	Laser powder bed fused Inconel 718 in stress-relieved and solution heat-treated conditions. Materials Characterization, 2021, 181, 111499.	4.4	16
24	Influence of sheet thickness ratio on fracture mechanisms of Al-steel resistance spot welds produced using multi-ring domed electrode. Science and Technology of Welding and Joining, 2020, 25, 164-168.	3.1	11
25	Microstructural investigation and mechanical behavior of a two-material component fabricated through selective laser melting of AlSi10Mg on an Al-Cu-Ni-Fe-Mg cast alloy substrate. Additive Manufacturing, 2020, 31, 100937.	3.0	26
26	Influence of build orientation on small-scale properties of electron beam melted Ti-6Al-4V. Materials Letters, 2020, 266, 126970.	2.6	13
27	Deformation mechanisms and fracture of electron beam melted Ti–6Al–4V. Materials Science & Engineering A: Structural Materials: Properties, Microstructure and Processing, 2020, 771, 138652.	5.6	27
28	Effects of Si, Mn on the corrosion behavior of ferritic–martensitic steels in supercritical water (SCW) environments. Corrosion Science, 2020, 166, 108432.	6.6	23
29	The role of titanium on the microstructure and mechanical properties of additively manufactured C300 maraging steels. Materials and Design, 2020, 194, 108965.	7.0	31
30	On the Joint Formation and Interfacial Microstructure of Cold Metal Transfer Cycle Step Braze Welding of Aluminum to Steel Butt Joint. Metallurgical and Materials Transactions A: Physical Metallurgy and Materials Science, 2020, 51, 5198-5212.	2.2	13
31	Wire-arc additive manufactured nickel aluminum bronze with enhanced mechanical properties using heat treatments cycles. Additive Manufacturing, 2020, 36, 101510.	3.0	15
32	On the solidification characteristics, deformation, and functionally graded interfaces in additively manufactured hybrid aluminum alloys. International Journal of Plasticity, 2020, 133, 102840.	8.8	25
33	Thermal–Mechanical Working of Spark Plasma Sintered Preforms Fabricated from Aluminum 2219 Powder. Metallurgical and Materials Transactions A: Physical Metallurgy and Materials Science, 2020, 51, 4647-4661.	2.2	2
34	On the Al–Al11Ce3 Eutectic Transformation in Aluminum–Cerium Binary Alloys. Materials, 2020, 13, 4549.	2.9	45
35	The Influence of Specimen Geometry and Strain Rate on the Portevin-Le Chatelier Effect and Fracture in an Austenitic FeMnC TWIP Steel. Metals, 2020, 10, 1201.	2.3	4
36	Interface engineering of additively manufactured maraging steel-H13 bimetallic structures. Materials Characterization, 2020, 170, 110728.	4.4	21

#	Article	IF	CITATIONS
37	Dynamic compressive response of electron beam melted Ti–6Al–4V under elevated strain rates: Microstructure and constitutive models. Additive Manufacturing, 2020, 35, 101347.	3.0	6
38	Additive manufacturing of an Fe–Cr–Ni–Al maraging stainless steel: Microstructure evolution, heat treatment, and strengthening mechanisms. Materials Science & Engineering A: Structural Materials: Properties, Microstructure and Processing, 2020, 787, 139470.	5.6	66
39	Generating C4 Alkenes in Solid Oxide Fuel Cells via Cofeeding H ₂ and <i>n</i> -Butane Using a Selective Anode Electrocatalyst. ACS Applied Materials & Interfaces, 2020, 12, 16209-16215.	8.0	15
40	Microstructural Evolution During Deformation of a QP980 Steel. Metallurgical and Materials Transactions A: Physical Metallurgy and Materials Science, 2020, 51, 4524-4539.	2.2	22
41	Micromechanical characterization of wire-arc additive manufactured and cast nickel aluminum bronze: Ambient and intermediate temperatures. Materials Science & Engineering A: Structural Materials: Properties, Microstructure and Processing, 2020, 792, 139773.	5.6	16
42	Microstructure and corrosion behavior of a novel additively manufactured maraging stainless steel. Electrochimica Acta, 2020, 339, 135925.	5.2	79
43	Microstructure evolution of warm deformed multilayered Al alloy sheet during brazing. Journal of Materials Processing Technology, 2020, 281, 116639.	6.3	14
44	A trade-off between powder layer thickness and mechanical properties in additively manufactured maraging steels. Materials Science & Engineering A: Structural Materials: Properties, Microstructure and Processing, 2020, 776, 139041.	5.6	53
45	Post heat treatment of additive manufactured AlSi10Mg: On silicon morphology, texture and small-scale properties. Materials Science & Engineering A: Structural Materials: Properties, Microstructure and Processing, 2020, 783, 139296.	5.6	80
46	Selective laser melted stainless steel CX: Role of built orientation on microstructure and micro-mechanical properties. Materials Science & Engineering A: Structural Materials: Properties, Microstructure and Processing, 2020, 786, 139365.	5.6	45
47	The Influence of Vanadium Additions on Isothermally Formed Bainite Microstructures in Medium Carbon Steels Containing Retained Austenite. Metals, 2020, 10, 392.	2.3	13
48	Microstructure and Shear Strength of Novel Aluminum to Steel Resistance Spot Welds. Welding Journal, 2020, 99, 67s-74s.	1.7	15
49	Corrosion Behaviour of Electron Beam Melted Ti6Al4V: Effects of Microstructural Variation. Journal of the Electrochemical Society, 2020, 167, 131505.	2.9	11
50	Additive manufacturing of maraging steel-H13 bimetals using laser powder bed fusion technique. Additive Manufacturing, 2019, 29, 100797.	3.0	58
51	Microstructural evolution and mechanical behavior of nickel aluminum bronze Cu-9Al-4Fe-4Ni-1Mn fabricated through wire-arc additive manufacturing. Additive Manufacturing, 2019, 30, 100872.	3.0	42
52	Using EELS-Carbon Measurement to Predict Hardness of V-added DP Steels. Microscopy and Microanalysis, 2019, 25, 2348-2349.	0.4	0
53	TEM Study of Additively Manufactured Metallic Alloys: Nickel Aluminum Bronze. Microscopy and Microanalysis, 2019, 25, 2588-2589.	0.4	3
54	High-Resolution Electron Microscopy and Kinetic Studies of Precipitation Hardening Reactions in Cast Al-5.8Zn-2.2Mg-2.5Cu. Journal of Materials Engineering and Performance, 2019, 28, 4630-4646.	2.5	5

#	Article	lF	CITATIONS
55	Microstructural assessment of 310S stainless steel during creep at 800°C. Materialia, 2019, 6, 100330.	2.7	8
56	Role of hierarchical microstructure of additively manufactured AlSi10Mg on dynamic loading behavior. Additive Manufacturing, 2019, 28, 1-13.	3.0	52
57	Evolution of a Gradient Microstructure in Direct Metal Laser Sintered AlSi10Mg. Minerals, Metals and Materials Series, 2019, , 331-338.	0.4	0
58	Microstructural evolution of a forged 2XXX series aluminum powder metallurgy alloy. Materials Characterization, 2019, 151, 342-350.	4.4	23
59	Friction stir lap welding of aluminum alloy to advanced high strength steel using a cold-spray deposition as an interlayer. Materials Letters, 2019, 239, 212-215.	2.6	18
60	Effect of coating type on microstructure and mechanical behavior of resistance spot welds of thin X626 aluminum sheet to low carbon steel. Journal of Materials Processing Technology, 2019, 264, 438-447.	6.3	23
61	Interfacial bonding mechanism in Al/coated steel dissimilar refill friction stir spot welds. Journal of Materials Science and Technology, 2019, 35, 1027-1038.	10.7	54
62	Contribution of Mg2Si precipitates to the strength of direct metal laser sintered AlSi10Mg. Materials Science & Engineering A: Structural Materials: Properties, Microstructure and Processing, 2019, 739, 295-300.	5.6	128
63	Deformation banding in a precipitation hardened aluminum alloy during simple shear deformation. Scripta Materialia, 2019, 162, 300-305.	5.2	19
64	Kinetics and microstructural change of low-carbon bainite due to vanadium microalloying. Materials Science & Engineering A: Structural Materials: Properties, Microstructure and Processing, 2018, 720, 248-256.	5.6	21
65	Promoting the ambient-condition stability of Zr-doped barium cerate: Toward robust solid oxide fuel cells and hydrogen separation in syngas. Journal of Power Sources, 2018, 378, 134-138.	7.8	19
66	Role of interfacial reaction on the mechanical performance of Al/steel dissimilar refill friction stir spot welds. Science and Technology of Welding and Joining, 2018, 23, 462-477.	3.1	30
67	Bimodal grain microstructure development during hot compression of a cast-homogenized Mg-Zn-Zr alloy. Materials Science & Engineering A: Structural Materials: Properties, Microstructure and Processing, 2018, 724, 421-430.	5.6	37
68	Deformation mechanism during dynamic loading of an additively manufactured AlSi10Mg_200C. Materials Science & Engineering A: Structural Materials: Properties, Microstructure and Processing, 2018, 722, 263-268.	5.6	44
69	Improvement of Superplasticity in High-Mg Aluminum Alloys by Sacrifice of Some Room Temperature Formability. Metallurgical and Materials Transactions A: Physical Metallurgy and Materials Science, 2018, 49, 1962-1979.	2.2	11
70	Forming mechanism of delamination cracks observed during tensile and fracture toughness testing of X70 pipeline steel. International Journal of Fracture, 2018, 209, 223-229.	2.2	3
71	Sagging resistance of warm formed aluminum brazing sheet. Journal of Materials Processing Technology, 2018, 254, 353-360.	6.3	15
72	Effect of Revolutionary Pitch on Interface Microstructure and Mechanical Behavior of Friction Stir Lap Welds of AA6082-T6 to Galvanized DP800. Metals, 2018, 8, 925.	2.3	9

#	Article	IF	CITATIONS
73	Activating p-Blocking Centers in Perovskite for Efficient Water Splitting. CheM, 2018, 4, 2902-2916.	11.7	99
74	Structure-properties relationship of ultra-fine grained V-microalloyed dual phase steels. Microscopy and Microanalysis, 2018, 24, 2232-2233.	0.4	0
75	Dynamic loading of direct metal laser sintered AlSi10Mg alloy: Strengthening behavior in different building directions. Materials and Design, 2018, 159, 201-211.	7.0	64
76	Liquid–Solid Interaction in Al-Si/Al-Mn-Cu-Mg Brazing Sheets and Its Effects on Mechanical Properties. Metallurgical and Materials Transactions A: Physical Metallurgy and Materials Science, 2018, 49, 3091-3107.	2.2	9
77	Strengthening mechanisms in direct metal laser sintered AlSi10Mg: Comparison between virgin and recycled powders. Additive Manufacturing, 2018, 23, 108-120.	3.0	110
78	Columnar to equiaxed transition during direct metal laser sintering of AlSi10Mg alloy: Effect of building direction. Additive Manufacturing, 2018, 23, 121-131.	3.0	90
79	Thermally stable and coking resistant CoMo alloy-based catalysts as fuel electrodes for solid oxide electrochemical cells. Journal of Materials Chemistry A, 2018, 6, 15377-15385.	10.3	21
80	New insights into martensite strength and the damage behaviour of dual phase steels. Acta Materialia, 2018, 159, 112-122.	7.9	36
81	The surface evolution of La0.4Sr0.6TiO3+ \hat{l}' anode in solid oxide fuel cells: Understanding the sulfur-promotion effect. Journal of Power Sources, 2017, 343, 127-134.	7.8	14
82	Interaction between nano-precipitates and dislocations during high temperature deformation of Al-Si alloys. Journal of Alloys and Compounds, 2017, 712, 219-224.	5.5	6
83	The role of the Zn/Nd ratio in the microstructural evolution of the Mg-Zn-Nd system during static recrystallization: Grain boundary partitioning of solutes. Scripta Materialia, 2017, 134, 1-5.	5.2	25
84	Effects of Heat-Affected Zone Microstructure on Fracture Toughness of Two X70 Pipe Girth Welds. Metallurgical and Materials Transactions A: Physical Metallurgy and Materials Science, 2017, 48, 3248-3260.	2.2	4
85	Quantitative metallography of precipitating and secondary phases after strengthening treatment of net shaped casting of Al-Zn-Mg-Cu (7000) alloys. Materials Science & Engineering A: Structural Materials: Properties, Microstructure and Processing, 2017, 698, 206-217.	5.6	62
86	Continuous nanoscale Al2Fe transition layer strengthened magnesium-steel spot joints. Materials Letters, 2017, 196, 242-244.	2.6	8
87	Structure-properties relationship of ultra-fine grained V-microalloyed dual phase steels. Materials Science & Engineering A: Structural Materials: Properties, Microstructure and Processing, 2017, 703, 293-303.	5.6	42
88	Characterization of oxide layer and micro-crack initiation in alloy 316L stainless steel after 20,000 h exposure to supercritical water at 500 ŰC. Materials Characterization, 2017, 131, 532-543.	4.4	16
89	Stabilizing Double Perovskite for Effective Bifunctional Oxygen Electrocatalysis in Alkaline Conditions. Chemistry of Materials, 2017, 29, 6228-6237.	6.7	94
90	Bonding mechanism and interface characterisation during dissimilar friction stir welding of an aluminium/polymer bi-material joint. Science and Technology of Welding and Joining, 2017, 22, 182-190.	3.1	63

#	Article	IF	CITATIONS
91	Internal oxidation and crack susceptibility of alloy 310S stainless steel after long term exposure to supercritical water at 500°C. Journal of Supercritical Fluids, 2017, 120, 161-172.	3.2	34
92	A comparative study on the oxidation of austenitic alloys 304 and 304-oxide dispersion strengthened steel in supercritical water at 650 ŰC. Journal of Supercritical Fluids, 2017, 119, 245-260.	3.2	43
93	Effect of Vanadium Addition on the Strength of API X100 Linepipe Steel. ISIJ International, 2016, 56, 154-160.	1.4	23
94	TEM Characterization of HSLA Steels and Welds. Microscopy and Microanalysis, 2016, 22, 1734-1735.	0.4	1
95	Effect of Weld Thermal Cycles on Microstructure and Properties of Simulated Heat Affected Zone in Thick-Wall X80 Pipe Steels. , 2016, , .		0
96	Hardness control of Al–Si HPDC casting alloy via microstructure refinement and tempering parameters. Materials and Design, 2016, 103, 365-376.	7.0	25
97	New Opportunity for <i>in Situ</i> Exsolution of Metallic Nanoparticles on Perovskite Parent. Nano Letters, 2016, 16, 5303-5309.	9.1	222
98	The Role of the Nd/Zn Ratio on the Stability of Mg-Zn-Nd Clusters and the Evolution of Texture in Two Mg-Zn-Nd Alloys during Annealing. Materials Science Forum, 2016, 879, 542-547.	0.3	0
99	Characterization of oxide scales grown on alloy 310S stainless steel after long term exposure to supercritical water at 500 ŰC. Materials Characterization, 2016, 120, 273-284.	4.4	31
100	Initiation of Stress Corrosion Cracks in X80 and X100 Pipe Steels in Near-Neutral pH Environment. Journal of Materials Engineering and Performance, 2016, 25, 227-240.	2.5	13
101	Mechanical Properties of Fuel Cladding Candidate Alloys for Canadian SCWR Concept. Jom, 2016, 68, 469-474.	1.9	11
102	Developing a Thermal- and Coking-Resistant Cobalt–Tungsten Bimetallic Anode Catalyst for Solid Oxide Fuel Cells. ACS Catalysis, 2016, 6, 4630-4634.	11.2	26
103	A comparative study of oxide scales grown on stainless steel and nickel-based superalloys in ultra-high temperature supercritical water at 800 ŰC. Corrosion Science, 2016, 106, 188-207.	6.6	121
104	TEM Examination of Precipitation Behaviour of M23C6 and Sigma Phases and Dislocations in SS 310S under Creep Deformation at 800°C. Microscopy and Microanalysis, 2015, 21, 585-586.	0.4	8
105	Effect of Vanadium Addition on Api X100 Linepipe Steel. , 2015, , 715-720.		0
106	Effect of water density on the oxidation behavior of alloy A-286 at 625°C – A TEM study. Journal of Nuclear Materials, 2015, 467, 758-769.	2.7	4
107	A-site deficient perovskite: the parent for in situ exsolution of highly active, regenerable nano-particles as SOFC anodes. Journal of Materials Chemistry A, 2015, 3, 11048-11056.	10.3	164
108	Microstructures and properties of Mg alloy/DP600 steel dissimilar refill friction stir spot welds. Science and Technology of Welding and Joining, 2015, 20, 494-501.	3.1	56

#	Article	IF	CITATIONS
109	An ingenious Ni/Ce co-doped titanate based perovskite as a coking-tolerant anode material for direct hydrocarbon solid oxide fuel cells. Journal of Materials Chemistry A, 2015, 3, 22830-22838.	10.3	42
110	Discovery and Understanding of the Ambient-Condition Degradation of Doped Barium Cerate Proton-Conducting Perovskite Oxide in Solid Oxide Fuel Cells. Journal of the Electrochemical Society, 2015, 162, F1408-F1414.	2.9	31
111	Microstructure and Toughness of Simulated Grain Coarsened Heat Affected Zones in X80 Pipe Steels. , 2014, , .		3
112	Microstructure-property characterization of a friction-stir welded joint between AA5059 aluminum alloy and high density polyethylene. Materials Characterization, 2014, 98, 73-82.	4.4	90
113	Formation of nanometer scale intermetallic phase at interface of aluminum-to-steel spot joint by welding–brazing process. Materials Letters, 2014, 137, 120-123.	2.6	17
114	Structure and properties of cast Al–Si based alloy with Zr–V–Ti additions and its evaluation of high temperature performance. Journal of Alloys and Compounds, 2014, 595, 67-79.	5.5	115
115	NbC Precipitation and Deformation of SS 347H Crept at 850°C. Microscopy and Microanalysis, 2014, 20, 1494-1495.	0.4	1
116	TEM Study of Supercritical Water Corrosion in 310S and 800H Alloys. Microscopy and Microanalysis, 2014, 20, 1866-1867.	0.4	8
117	Thermodynamically destabilized hydride formation in "bulk―Mg–AlTi multilayers for hydrogen storage. Physical Chemistry Chemical Physics, 2013, 15, 16432.	2.8	12
118	Supercapacitors based on carbons with tuned porosity derived from paper pulp mill sludge biowaste. Carbon, 2013, 57, 317-328.	10.3	155
119	Magnesium and magnesium-silicide coated silicon nanowire composite anodes for lithium-ion batteries. Journal of Materials Chemistry A, 2013, 1, 1600-1612.	10.3	52
120	Graphene-nickel cobaltite nanocomposite asymmetrical supercapacitor with commercial level mass loading. Nano Research, 2012, 5, 605-617.	10.4	356
121	Electrochemical Supercapacitor Electrodes from Sponge-like Graphene Nanoarchitectures with Ultrahigh Power Density. Journal of Physical Chemistry Letters, 2012, 3, 2928-2933.	4.6	173
122	Supercapacitive carbon nanotube-cobalt molybdate nanocomposites prepared via solvent-free microwave synthesis. RSC Advances, 2012, 2, 2753.	3.6	113
123	Stable Hydrogen Storage Cycling in Magnesium Hydride, in the Range of Room Temperature to 300 °C, Achieved Using a New Bimetallic Cr-V Nanoscale Catalyst. Journal of Physical Chemistry C, 2012, 116, 3188-3199.	3.1	54
124	Carbonized Chicken Eggshell Membranes with 3D Architectures as Highâ€Performance Electrode Materials for Supercapacitors. Advanced Energy Materials, 2012, 2, 431-437.	19.5	573
125	Carbonized Chicken Eggshell Membranes with 3D Architectures as High-Performance Electrode Materials for Supercapacitors (Adv. Energy Mater. 4/2012). Advanced Energy Materials, 2012, 2, 430-430.	19.5	10
126	Microstructural evolution during low temperature sorption cycling of Mg-AlTi multilayer nanocomposites. International Journal of Hydrogen Energy, 2012, 37, 4215-4226.	7.1	18

#	Article	IF	CITATIONS
127	Microstructural evolution during hydrogen sorption cycling of Mg–FeTi nanolayered composites. Acta Materialia, 2011, 59, 2083-2095.	7.9	37
128	Synergy of elemental Fe and Ti promoting low temperature hydrogen sorption cycling of magnesium. International Journal of Hydrogen Energy, 2011, 36, 6711-6722.	7.1	51
129	Bimetallic Fe–V catalyzed magnesium films exhibiting rapid and cycleable hydrogenation at 200 °C. Applied Physics Letters, 2010, 96, .	3.3	24
130	Hydrogen storage cycling of MgH2 thin film nanocomposites catalyzed by bimetallic Cr Ti. Applied Physics Letters, 2010, 97, .	3.3	54
131	Hydrogen Sorption Cycling Kinetic Stability and Microstructure of Single-Walled Carbon Nanotube (SWCNT) Magnesium Hydride (MgH ₂) Nanocomposites. Journal of Physical Chemistry C, 2010, 114, 3265-3275.	3.1	63
132	Rapid and reversible hydrogen sorption in Mg–Fe–Ti thin films. Applied Physics Letters, 2009, 95, 103114.	3.3	49
133	The influence of SWCNT–metallic nanoparticle mixtures on the desorption properties of milled MgH ₂ powders. Nanotechnology, 2009, 20, 204016.	2.6	60
134	Nano-scale bi-layer Pd/Ta, Pd/Nb, Pd/Ti and Pd/Fe catalysts for hydrogen sorption in magnesium thin films. International Journal of Hydrogen Energy, 2009, 34, 7741-7748.	7.1	54
135	Characterisation of phase segregation during back extrusion of ZA27 semisolid alloy. Materials Science and Technology, 2007, 23, 113-118.	1.6	4
136	Phase Segregation Susceptibility of ZA27 Alloy at Different Shear Rates. Solid State Phenomena, 2006, 116-117, 225-230.	0.3	1
137	Joining Metals by Combining Mechanical Stirring and Thermomechanical Treatment to Form a Globular Weld Structure. Solid State Phenomena, 2006, 116-117, 397-401.	0.3	17
138	The influence of the ratio of "rotational speed/traverse speed―(ω/v) on mechanical properties of AZ31 friction stir welds. International Journal of Machine Tools and Manufacture, 2006, 46, 1983-1987.	13.4	138
139	Evaluation of microstructure and mechanical properties in friction stir welded A356+15%SiCp cast composite. Materials Letters, 2006, 60, 565-568.	2.6	95
140	Joining Metals by Combining Mechanical Stirring and Thermomechanical Treatment to Form a Globular Weld Structure. Solid State Phenomena, 0, , 397-401.	0.3	0
141	On the Microstructure and Solidification Behavior of a Novel Additively Manufactured Al-Cu-Mg-Ag-Ti-B Alloy. SSRN Electronic Journal, 0, , .	0.4	0
142	Characterization and Statistical Modeling of Texture and Microstructure Evolution in Dynamically Fractured Electron Beam Melted Ti-6Al-4V. SSRN Electronic Journal, 0, , .	0.4	0
143	High Strain Rate Deformation Behavior, Texture and Microstructural Evolution, Characterization of Adiabatic Shear Bands, and Constitutive Models in Electron Beam Melted Ti-6al-4v Under Dynamic Compression Loadings. SSRN Electronic Journal, 0, , .	0.4	0